Individual clinical advanced decision-making and risk evaluation for Ewing sarcoma

Bosma, S.E.

PART II

Pre-operative and intra-operative imaging techniques

CHAPTER 5

^{18}F-FDG PET-CT versus MRI for detection of skeletal metastasis in Ewing sarcoma.

S.E. Bosma, D. Vriens, A.J. Gelderblom, M.A.J. van de Sande, P.D.S. Dijkstra, J.L. Bloem

Skeletal Radiology 2019 Apr 23

Abstract

Objective
To determine the level of discrepancy between magnetic resonance imaging (MRI) and ^{18}F-FDG PET-CT in detecting osseous metastases in patients with Ewing sarcoma.

Methods
20 patients with histopathological confirmed Ewing sarcoma between 2000 and 2017 who had ^{18}F-FDG PET-CT and MRI performed within a 4-week range were included. Each imaging modality was evaluated by a separate observer. Reference diagnosis of each lesion was based on histopathology or consensus of an expert panel using all available data, including at least 6 months follow-up. Sensitivity, specificity, and predictive values were determined. Osseous lesions were analyzed on patient- and lesion-basis. Factors possibly related to false-negative findings were evaluated using Pearson's chi-square of Fisher's exact test.

Results
112 osseous lesions were diagnosed in 13 patients, 107 malignant and five benign. Seven patients showed no metastases on either ^{18}F-FDG PET-CT or MRI. Forty-one skeletal metastasis (39%) detected with MRI did not show increased ^{18}F-FDG uptake on ^{18}F-FDG PET-CT (false-negative). Lesion-based sensitivities and specificities were 62% (95%CI 52-71%) and 100% (48-100%) for ^{18}F-FDG PET-CT; and 99% (97-100%) and 100% (48-100%) for MRI, respectively. Bone lesions were more likely to be false-negative on ^{18}F-FDG PET-CT if hematopoietic bone marrow extension was widespread and active ($p=0.001$), during or after (neo)-adjuvant treatment ($p=0.001$) or when the lesion was smaller than 10 mm ($p<0.001$).

Conclusion
Although no definite conclusions can be drawn from this small retrospective study, it shows that caution is needed when using ^{18}F-FDG PET-CT for diagnosing skeletal metastases in Ewing sarcoma. Poor contrast between metastases and active hematopoietic bone marrow, chemotherapeutic treatment and/or small size significantly decrease the diagnostic yield of ^{18}F-FDG PET-CT, but not of MRI.

Introduction

Ewing sarcoma is an aggressive primary bone sarcoma, predominantly affecting children and young adults.(1, 2) At the time of diagnosis, 20 to 25% of the patients present with pulmonary (70-80%) and/or osseous (40-50%) metastases. A multimodal approach to treatment drastically improved survival. In non-metastatic Ewing sarcoma 10-year overall survival is currently 55 to 65%, but survival in metastatic Ewing sarcoma is still dismal, with a 5-year overall survival of only 20 to 35%. (3-5) Principles of treatment consist of neo-adjuvant chemotherapy followed by local control of the primary tumor, either by surgery, radiotherapy or both, and adjuvant chemotherapy. (2, 4) Detection of all metastatic lesions in patients with oligometastatic disease has become relevant, as a curative rather than a palliative treatment objective aimed at achieving local control at these sites has been reported to improve clinical outcome. (6) Pre-treatment imaging of newly diagnosed patients with Ewing sarcoma includes local staging with magnetic resonance imaging (MRI) and chest computerized tomography (CT) to detect pulmonary metastases (15). Bone marrow biopsies and bone scintigraphy have been used to detect or exclude skeletal metastases. More recently 2-[^{18}F]fluoro-2-deoxy-D-glucose positron emission tomography with CT (^{18}F-FDG PET-CT) and whole-body MRI have been proposed to replace bone scintigraphy, because of higher sensitivity, and thus negative predictive value, to exclude skeletal metastasis. (7-12) With ^{18}F-FDG PET-CT reflecting glucose metabolism of the lesions and MRI imaging revealing morphologic characteristics of metastatic deposits, these two screening techniques display different properties of the cancerous lesions: either functional or anatomical. No published literature directly comparing ^{18}F-FDG PET-CT with whole-body MRI for detection of skeletal metastases in Ewing sarcoma is currently available. Literature comparing both modalities for skeletal metastases in other cancers shows conflicting results, with some suggesting superiority for ^{18}F-FDG PET-CT (10, 13, 14) and others superiority for MRI. (7, 15)

In our clinical practice we normally use both techniques. We frequently observed a mismatch between ^{18}F-FDG PET-CT and MRI; in some patients, metastatic skeletal lesions detected by MRI were not detected with ^{18}F-FDG PET-CT. Therefore, our purpose of this study was to retrospectively compare the diagnostic yield of ^{18}F-FDG PET-CT to whole-body MRI for detection of skeletal metastasis in Ewing sarcoma with final diagnosis of an osseous lesion made by an expert panel using all follow-up data or histopathology (where available).

Methods

Study design and patients

The local ethical board approved this retrospective study and waived the requirement for informed consent. We searched the database of our tertiary referral bone sarcoma center for all patients diagnosed with Ewing sarcoma between the

first of January 2010 and the first of January 2018. Patients were eligible for inclusion when fulfilling all of the following criteria: 1) histopathological confirmed Ewing sarcoma; 2) treatment and diagnostic work-up according to the EURO-E.W.I.N.G. (EUROpean Ewing tumor Working Initiative of National Groups-Ewing Tumour Studies) 2008 or 2012 protocol; 3) whole-body ^{18}F-FDG PET-CT scan and whole body or large field of view regional MRI scan performed within a 4-week range. All sets of scans performed at baseline were executed before the start of treatment. All sets of scans performed during follow-up were executed at the same treatment stage or moment in follow-up. In case of multiple paired ^{18}F-FDG PET-CT and MRI scans of a single patient, the first available set was used. We performed an additional analysis for therapy naïve patients and patients who were already treated separately to check if this had an impact on detection.

We identified 52 patients with histopathological confirmed Ewing sarcoma and included 20 patients who had undergone both ^{18}F-FDG PET-CT scan and MRI scan, either at diagnosis or during follow-up, within a 4-week range.

Figure 1 shows a flowchart of the inclusion process.

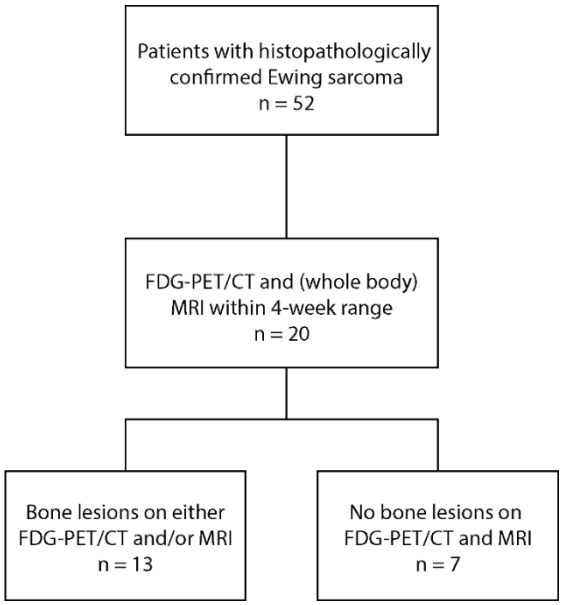

Figure 1 - Flowchart of the inclusion process

^{18}F-FDG PET-CT acquisition and evaluation

After at least six hours of fasting (sugar-free liquids were allowed) and validation of normoglycemia (<11.1 mmol/L), patients were intravenously injected with ^{18}F-FDG (dose dependent on bodyweight, scanner sensitivity and acquisition duration). After a ~60-minute resting period, low-dose CT and PET-images were acquired from vertex to toes on multiple PET-CT scanners (Siemens Biograph Horizon, Siemens Biograph mCT and Philips Gemini TF) in our own and six referring centers according to the European Association of Nuclear Medicine (EANM) procedure guidelines for tumor imaging in FDG PET-CT (version 2.0). (16) Analysis of ^{18}F-FDG PET-CT-images was repeated for all scans and primarily done by visual assessment. The decision of the conspicuity of a skeletal lesion was determined by an experienced PET-CT-reader (D.V., nuclear medicine physician, 10 years of experience), blinded for clinical and histopathological information and other imaging examinations. Visible lesions on ^{18}F-FDG PET-CT were scored positive (i.e. suspect for malignancy), negative (i.e. suspected benign) or inconclusive. Focal bone uptake visual in thee orthogonal plans, higher than the surrounding bone marrow without clear benign cause (e.g. growth plate) was scored as suspect for malignancy (positive). In case additional imaging was suggested for confirmation, it was scored as 'inconclusive'. All other lesions were scored benign (negative). Semi quantitative assessment of PET-positive lesions by measurement of their maximum standardized uptake value (SUV_{max}) was performed and related to the SUV_{max} of the mediastinal blood pool and healthy right liver activity, resulting in the 6-point scale presented in Table 1. Last, metabolically active hematopoietic bone marrow extension and activity was quantified using a visual 4-point scale defined *a priori* based on literature. (17-19) The visual 4-point scale was defined as followed: 0) metabolically active hematopoietic bone marrow only present in spine/pelvis without increased activity (SUV_{max} lower than or equally to liver); 1) metabolically active hematopoietic bone marrow only present in spine/pelvis with increased activity (SUV_{max} higher than the liver); 2) metabolically active hematopoietic bone marrow extension up to pertrochanteric femoral and/or subcapital humeral regions with increased activity; 3) metabolically active hematopoietic bone marrow extension beyond pertrochanteric femoral and/or subcapital humeral regions with increased activity. For analysis we dichotomized the data, normal hematopoietic bone marrow was defined by a score of 0 or 1 and widespread hematopoietic bone marrow extension and activity was defined as a score of 2 or 3.

Score	Description
0	No uptake
1	Notable uptake < mediastinal blood pool
2	Notable uptake > mediastinal blood pool, but < liver
3	Notable uptake ≈ liver uptake (±10%)
4	Intense uptake > liver, but ≤ 2,5x liver
5	Intense uptake > 2.5x liver uptake

Table 1 – Semi-quantitative assessment of lesion ^{18}F-FDG uptake according to a 6-point scale.

MRI acquisition and evaluation

Whole body MRI was performed in 14 patients using a 1.5T system (Philips Healthcare, Best, the Netherlands). Standard protocol included T1-weighted turbo spin echo (TSE) with slice thickness: 5 mm, repetition time (TR) of 727 ms, echo time (TE) of 15 ms, and short-Tau inversion recovery (STIR) sequences using four stations in the coronal plane with slice thickness: 5 mm , TR 7192 ms, TE 50 ms, inversion time 210 m, and sagittal T1 and STIR sequences of the entire spine using the above mentioned MRI parameters for T1 and STIR. In six patients a large field of view regional MRI scan using the same parameters was obtained. Additional sequences that were made in these regional scans were not reviewed for current analysis. In these six patients, only regions imaged by both modalities were evaluated and compared. In one of these six patients, ^{18}F-FDG PET-CT showed three osseous lesions outside the MRI field of view, which were not included for current analysis.

MRI images were evaluated by one radiologist specialized in MRI imaging (J.L.B., >10 years of experience), blinded for clinical and histopathological information and other imaging examinations. Malignancy on MRI was based on the assessment of morphological and signal characteristics. A nodule presenting with a lower signal than the surrounding bone marrow on T1 and a higher signal on STIR sequences was scored positive (i.e. suspect for malignancy). All other lesions were considered benign (negative). Next, quantitative assessment of MRI positive lesions was performed by measuring the size (defined as maximum diameter) of the lesion. Lesions were dichotomized at the 10mm diameter level.

Reference method

Histopathological correlation for every depicted osseous lesion was not available in the majority of the lesions for ethical reasons: in only two patients, confirmation of skeletal metastasis by biopsy was available. In the other 11 patients with osseous lesions on imaging, the final decision of the true status of the osseous lesion was made by consensus using an expert panel consisting of a board-certified radiologist and nuclear physician. All available clinical information, including therapy schedules, response to treatment and follow-up imaging examinations (^{18}F-FDG PET-CT, MRI, diagnostic CT) were used to reach the overall decision. Patients were routinely evaluated every 3 months by ^{18}F-FDG PET-CT and/or MRI. The mean imaging follow-up was 15,7 months (range 1,8 to 31,3 months). Two patients deceased due to progressive disease shortly (1,8 and 3,8 months) after imaging was performed and no obduction was performed. In all other 18 patients (7 without osseous lesions and 11 with osseous lesions) at least 6 months of follow-up imaging examinations was available to determine the true status of a bone lesion. Change in imaging characteristics, increase in size of the entire lesion or the extra-osseous component or increased ^{18}F-FDG uptake of the lesions indicated malignancy. Response to treatment was used as a sign of malignancy and was defined as decrease in ^{18}F-FDG-uptake, decrease in size of the lesions or complete disappearance of the lesion. A lesion was considered benign if a specific diagnosis could be made, if it showed no change over time, especially when other lesions changed in response to treatment, or if there was progressive disease diagnosed in other sites of the skeleton.

Data analysis

Each visible lesion was scored separately as being malignant, benign or inconclusive on either imaging modality. Number of lesions and location were determined for both ^{18}F-FDG PET-CT and MRI. Location was defined using eleven predefined skeletal body regions: 1) skull; 2) ribs; 3) pelvis; 4) cervical spine; 5) thoracic spine; 6) lumbar spine; 7) proximal upper extremity; 8) distal upper extremity; 9) proximal lower extremity; 10) distal lower extremity; 11) other regions (scapula, sternum, clavicles). If a patient presented with multiple lesions in one region a maximum of 4 lesions was included for analysis to avoid bias of few patients with very large number of lesions. In case of discordance between ^{18}F-FDG PET-CT and MRI, we searched for potential causes in a separate consensus meeting by the expert panel, after all patients had been scored by the individual observers. Additionally, if osseous lesions showed no ^{18}F-FDG uptake we evaluated whether these lesions were visible on the low-dose CT of the ^{18}F-FDG PET-CT, using MRI as guidance.

Statistical analysis

Both patient-based analysis and lesion-based analysis were performed and the results are described as true-positive, true-negative, false-positive and false-negative. Lesions that were scored as inconclusive on imaging were considered

positive for this analysis. Osseous lesions were also evaluated and reported as true-positive, false-positive, true-negative, and false-negative in patient-based and lesion-based analysis. In case of a discordant finding within a single patient, a true-positive lesion will supersede all other lesions, including false-negative, true-negative and false-positive lesions. Thus, if a subject presented with at least one true-positive lesion, that patient will be considered true-positive for this imaging modality. In the absence of a true-positive lesions, a false-negative lesion will supersede a true-negative or false-positive lesion. Therefore, if imaging is false-negative in at least one site, that patient will be considered false-negative overall for this modality. Using this approach, we address the question if recurrent/metastatic disease is present or not. We computed accuracy, sensitivity, specificity, positive and negative predictive values using the classical equations. The 95%-confidence intervals of these test characteristics were computed using the absolute Clopper-Pearson interval (using the beta-distribution). We explored the following factors to be related to false-negative findings: lesion size, location, hematopoietic bone marrow extension and treatment stage (before treatment, on treatment, recurrence after treatment) using Pearson's chi-square or Fisher's exact test, where appropriate.

Results

Patient population

In seven of the 20 patients ^{18}F-FDG PET-CT and MRI were both negative for the presence of osseous lesions. All these patients were routinely evaluated every 3 months by ^{18}F-FDG PET-CT and MRI and none of these patients was diagnosed with skeletal metastasis within the next six months. All these cases were considered true-negative on both imaging modalities. Later three of these patients developed pulmonary and/or skeletal metastasis during long term follow-up. At the termination of our study, the four other patients were alive with no evidence of disease and the three patients who later developed metastases, died due to recurrent or progressive disease.

In the remaining 13 patients, Table 2, osseous lesions on any or both imaging modalities were reported to be present. A total of 112 bone lesions were identified using our standard of reference; 89 in the axial skeleton (30 vertebral, 15 rib, 33 pelvic, 4 glenoid, 1 acromion, 3 clavicles, 2 sternum, 1 skull), and 23 in the peripheral skeleton (16 lower extremity, 7 upper extremity). Four patients had already been treated at the time of imaging, while all imaging was performed prior to start of treatment in the other nine patients. At the termination of our study seven patients had died due to progressive disease, six patients were alive of which four were undergoing palliative treatment and two were alive with no evidence of disease.

						^{18}F-FDG PET-CT		MRI	
No.	**Age/Sex**	**Primary tumor**	**Purpose of the study**	**Standard of reference**	**Number of lesions#**	**PB**	**LB**	**PB**	**LB**
1	23/M	Tibia	Follow-up*	CF	16	TP	6	TP	16
2	22/M	Femur	Follow-up	CF	2	TP	2	TP	2
3	23/M	Femur	Staging	CF	3	TP	3	TP	3
4	26/M	Pelvic	Staging	CF	25	TP	19	TP	24
5	17/M	Tibia	Follow-up	CF	16	TP	6	TP	16
6	17/F	Costa	Follow-up	CF	2	FP	2	TN	0
7	5/F	Tibia	Staging	HP	1	TP	1	TP	1
8	23/M	Humerus	Staging	CF	24	TP	19	TP	23
9	8/F	Tibia	Staging	HP	2	TP	1	TP	2
10	23/M	Costa	Staging	CF	11	TP	4	TP	11
11	22/M	Pelvic	Staging	CF	5	TP	3	TP	5
12	16/M	Fibula	Staging	CF	1	TP	1	TP	1
13	29/F	Femur	Staging	CF	2	TP	2	TP	2
Total					**112**		**69**		**106**

Table 2 - Patient-based and lesion-based diagnosis of bone lesions in patients with at least one abnormality

Abbreviations: CF = clinical follow-up; F = female; FN = false negative; FP = false positive; HP = histopathology; LB = lesion based positive lesions; M = male; PB = patient basis; TP = true positive; TN=true negative

**active chemotherapeutic treatment*

#on any of both imaging modalities

Patient-based analysis for PET-CT vs MRI

Twelve out of 13 patients (92.3%) with suspicion of skeletal metastasis on any of the two imaging modalities were correctly identified by ^{18}F-FDG PET-CT and MRI concordantly, and thus were considered true positive.

In one patient (7.7%) ^{18}F-FDG PET-CT showed two almost symmetric lesions with subtle sclerosis and ^{18}F-FDG-uptake in both distal femoral diaphysis of which the true nature could not be clearly defined. Based on the information available these lesions were classified as inconclusive. On MRI and CT a diagnosis of bilateral bone infarctions was made as confirmed by the expert panel (Figure 2). During follow-up the patient presented with progressive disease, and eventually died 16.3 months later. No metastatic lesions developed at the distal femora during the disease progression and the bone infarctions didn't change, the ^{18}F-FDG PET-CT was therefore considered false-positive. There were no false-positive MRI-scans and there were no false-negative scans. The positive predictive values (PPV) with corresponding 95%-confidence interval (95%CI) of ^{18}F-FDG PET-CT and MRI therefore were respectively 92% (62-100%) and 100% (72-100%), respectively. The sensitivities were 100% (72-100%) for ^{18}F-FDG PET-CT and 100% (72-100%) for MRI.

Lesion-based analysis

A total of 112 lesions in 13 patients were identified and characterized as malignant or benign by the expert panel using the predefined standard of reference. Of these 112, 107 lesions (95.5%), present in 12 patients, were considered malignant . Five lesions in four patients were considered to be benign.The data from the lesion-based analysis are presented in Table 3.

^{18}F-FDG PET-CT and MRI were concordantly positive in 65 (58%) osseous lesions, whereas 41 (37%) osseous lesions in seven patients were observed on MRI only, compared to 4 (4%) osseous lesions in three patients observed on ^{18}F-FDG PET-CT only. Two osseous lesions (1%) in one patient were defined as being benign on both imaging modalities.

		PET		
		+	-	Total
MRI	+	65	41	106
	-	4	2	6
	Total	69	43	112

Table 3 – Lesion-based analysis of all osseous lesions.

The 41 lesions visible on MRI only were all considered to be malignant according to the standard of reference and therefor true-positive. These 41 lesions were thus false-negative on ^{18}F-FDG PET-CT. The majority of these 41 lesions (36 lesions; 88%) was located in the axial skeleton; spine (20 lesions; 49%), rib (2 lesions; 5%), pelvis (7 lesions; 17%), other axial regions (glenoid and clavicles; 7 lesions, 17%). Only 5 lesions (12%) were found in the extremities. Lesions were not more likely to be false-negative on ^{18}F-FDG PET-CT when located in the axial skeleton compared to an extremity location (40% versus 30%; p=0.522). In addition to location in the axial skeleton we evaluated potential cofounders potentially explaining the false-negative lesions on ^{18}F-FDG PET-CT. In the nine therapy-naïve patients, lesions were less likely to be false-negative on ^{18}F-FDG PET-CT compared to the four patients that already started treatment (26% versus 58%; p=0.001). In three patients with false-negative lesions on ^{18}F-FDG PET-CT widespread hematopoietic bone marrow extension and activity was present. Lesions were more likely to be false-negative on ^{18}F-FDG PET-CT when widespread active red bone marrow was present (55% versus 22%, p=0.001). In one patient recent chemotherapy led to bone marrow rebound on ^{18}F-FDG PET-CT obscuring ten lesions all located in the axial skeleton (Figure 3). Ten lesions in five patients were smaller than 10 mm and all but one of these lesions were located in the axial skeleton. Lesion size below 10 mm lead to more false-negative lesions on ^{18}F-FDG PET-CT (100% versus 30%, p<0.001). Figure 4 and 5 provide examples of the false negative lesions on ^{18}F-FDG PET-CT.

Of these 41 false negative lesions on ^{18}F-FDG PET-CT, 39 could not be identified on the low-dose CT of the ^{18}F-FDG PET-CT by the expert panel. The expert panel identified two skeletal metastasis present in two patients that were visible on the low-dose CT as small osteolytic lesions, positive on MRI but interpreted as negative on ^{18}F-FDG PET-CT. One of these two false-negative lesions, was in close proximity to the physiologically ^{18}F-FDG positive growth plate and (thus) falsely interpreted as negative. The other false-negative lesion was located at the in the posterior iliac crest and interpreted as reactive uptake due to bone-marrow biopsy for its location. However, no bone marrow biopsy had been performed, and the small lytic lesion on low-dose CT had been interpreted as iatrogenic. All other 39 false-negative lesions showed no ^{18}F-FDG uptake on PET-CT. On MRI and during imaging follow-up this lesion was classified as malignant and thus interpreted false-negative by ^{18}F-FDG PET-CT.

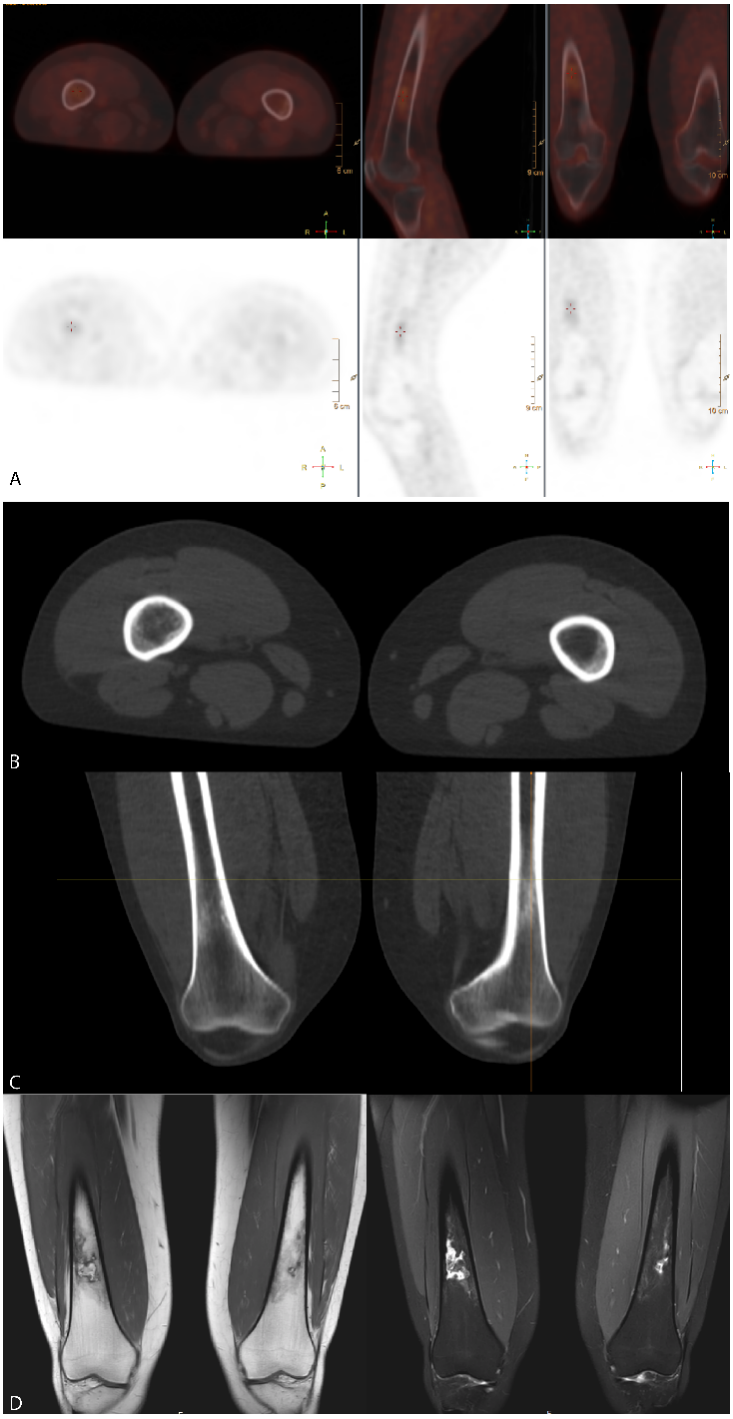
A
B
C
D

Figure 2 - False-positive lesions on 18F-FDG PET-CT.
A 19-year-old woman diagnosed with localized Ewing sarcoma of the seventh rib. Six months after initial treatment consisting of six courses of vincristine, ifosfamide, doxorubicin, and etoposide (VIDE) chemotherapy, 8 courses of vincristine, actinomycin-D, and ifosfamide (VAI) chemotherapy, radiation therapy and surgery, imaging was performed because of chest pain, with local recurrence suspected. A) 18F-FDG PET-CT showed two lesions with 18FDG-uptake in both femora of which the true nature could not be clearly defined; based on the information available they were classified as inconclusive (positive). B) and C) Low-dose CT images in the transverse and coronal planes of the suspected bone lesions showing sclerosis. d MRI T1- and T2-weighted images show bilateral bone infarctions and no sign of malignancy

Three out of four bone lesions visible on ^{18}F-FDG PET-CT only, were considered false-positive. These included two lesions diagnosed as bone infarctions in a single patient (Fig 1) and a bone lesion in the 8th thoracic vertebral body. During imaging follow-up of over a year no change of the lesion in the 8th thoracic vertebral body was seen. A diagnosis could not be made, however since no progression or change of the lesion was seen in over a year, while the patient had progressive disease under treatment, the lesion was regarded as being benign according to our reference standard and therefor as false-positive on ^{18}F-FDG PET-CT.
The one PET-positive lesion that was false-negative on MRI according to the standard of reference was missed due to partial volume effects. This small lesion (<1 cm) fell between two slices due to the slice gap of 10% with a slice thickness of 5 mm.
Table 4 provides an overview of the lesion-based analysis relative to the standard of reference for each imaging modality separately. The lesion-based PPV for ^{18}F-FDG PET-CT and MRI were respectively 96% (95%CI 91-100%) and 100% (97-100%). The lesion-based NPV for ^{18}F-FDG PET-CT and MRI were respectively 5% (0-11%) and 83% (54-100%). Sensitivities and specificities for these modalities were 62% (95%CI 52-71%) and 100% (95%CI 48-100%) for ^{18}F-FDG PET-CT and 99% (97-100%) and 100% (48-100%) for MRI, respectively. Accuracy was 63% (95%CI 54-72%) for ^{18}F-FDG PET-CT and 99% (95%CI 95-100%) for MRI.

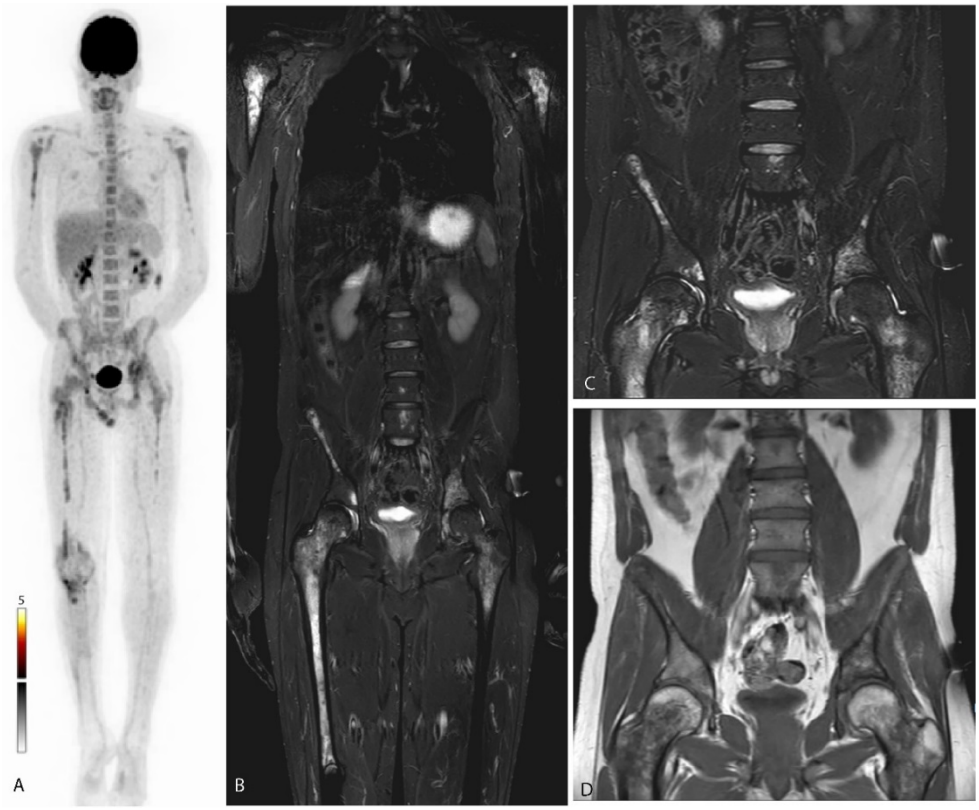

Figure 3 - False-negative lesions on 18F-FDG PET-CT with widespread hematopoietic bone marrow activity.

A 23-year-old man diagnosed with localized Ewing sarcoma of the right proximal tibia. Images obtained 6 months after initial treatment (6 × VIDE, surgery, 8 × VAI), at this time undergoing second-line chemotherapy because of recent distant metastasis. A) 18F-FDG PET-CT with symmetrical 18F-FDG uptake in the axial skeleton and proximal extremities. This was classified benign (negative) owing to anemia or recent chemotherapy. B) T1-weighted short tau inversion recovery (STIR) MRI images with multifocal metastatic lesions throughout the whole axial skeleton. C) STIR images with several skeletal metastases in the left and right ilium and fifth lumbar vertebral body. D) T1-weighted turbo spin echo (TSE) images with several skeletal metastases in the left and right ilium and fifth lumbar vertebral body

		Standard of reference	
		Malignant	**Benign**
PET	**+**	66	0
	-	41	2
	Indeterminate	0	3
MRI	**+**	106	0
	-	1	5

Table 4 – Lesion based analysis according to the standard of reference.

Semi quantitative assessment of ^{18}F-FDG PET-CT
Most of the true positive PET lesions (67/107, 63%) had a score of 3 (notable uptake with a SUV_{max} of ±10% compared to the liver uptake) or higher. The remaining 40 lesions showed no visible uptake on ^{18}F-FDG PET-CT or only showed low uptake and were considered as benign (SUV_{max} lower than bloodpool). See table 5.

			Score					
		total	**0**	**1**	**2**	**3**	**4**	**5**
Standard of reference	Malignant	107	36	2	2	3	52	12
	Benign	5	0	0	2	0	3	0
PET-CT interpretation	Positive/Indeterminate	69	0	0	4	2	53	10
	Negative	43	36	2	0	1	2	2

Table 5 – Scores of ^{18}F-FDG PET-CT lesions
Score based on maximum SUV_{max} divided into standard of reference and visual ^{18}F-FDG PET-CT interpretation.

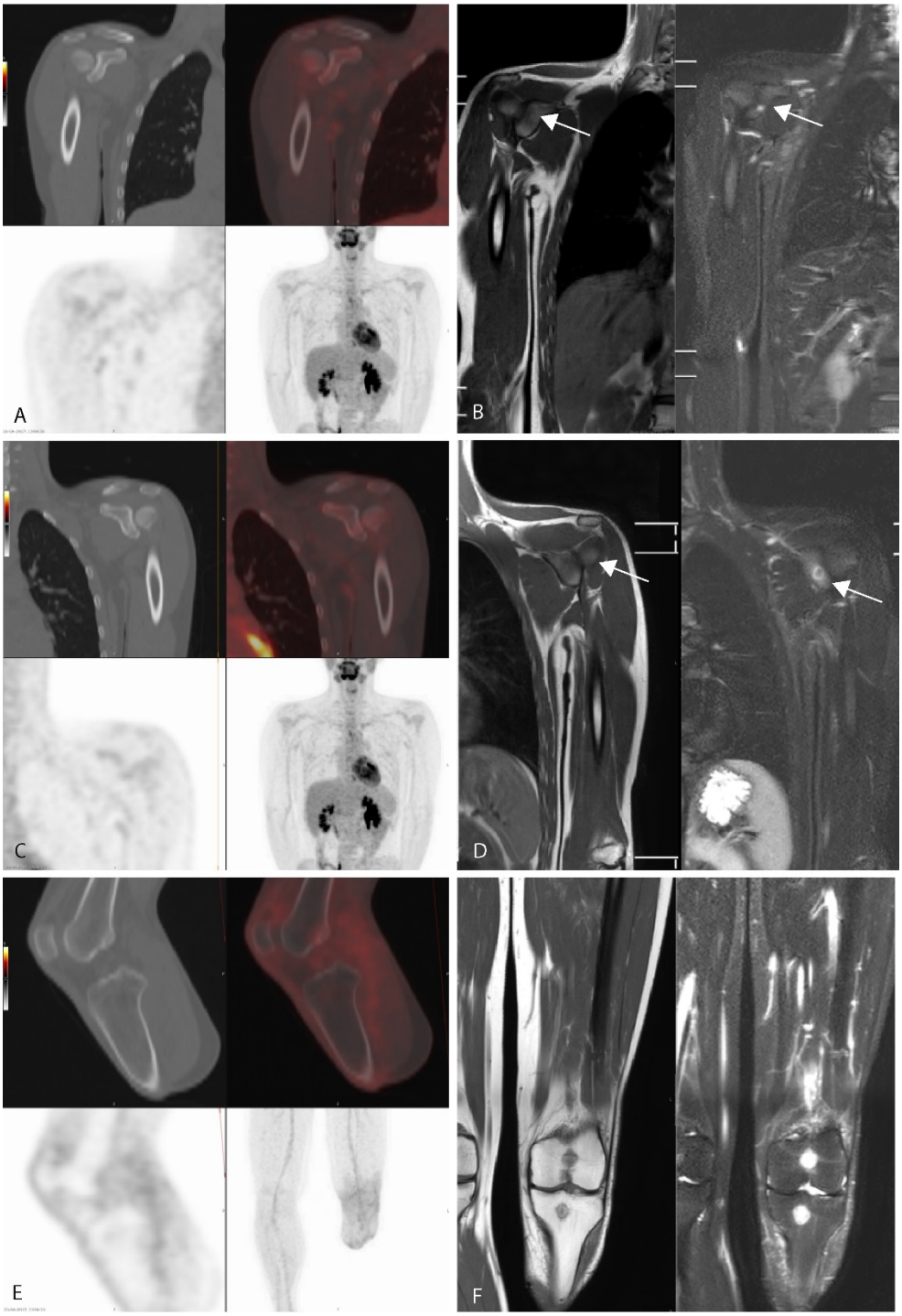
A
B
C
D
E
F

Figure 4 - False-negative lesions on 18F-FDG PET-CT.
A 17-year-old boy diagnosed with localized Ewing sarcoma of the distal tibia. Images obtained 1 year after finishing treatment (6 × VIDE, amputation, 8 × VAI). A) 18F-FDG PET-CT showing no increased 18F-FDG-uptake at the glenoid of the right shoulder. B) T1-weighted (left) and STIR (right) images showing a small nodule (arrow) with a high degree of suspicion for metastasis at the glenoid of the right shoulder. C) 18F-FDG PET-CT showing no increased 18F-FDG-uptake or lytic changes on low-dose CT at the glenoid of the left shoulder. D) T1-weighted (left) and STIR (right) images showing a nodule (arrow) with a high degree of suspicion for metastasis at the glenoid of the left shoulder. E) 18F-FDG PET-CT showing no increased 18F-FDG-uptake or lytic changes on low-dose CT at the left proximal tibia and distal femur. F) T1-weighted (left) and STIR (right) images showing two nodules with a high degree of suspicion for metastasis at the left proximal tibia and distal femur

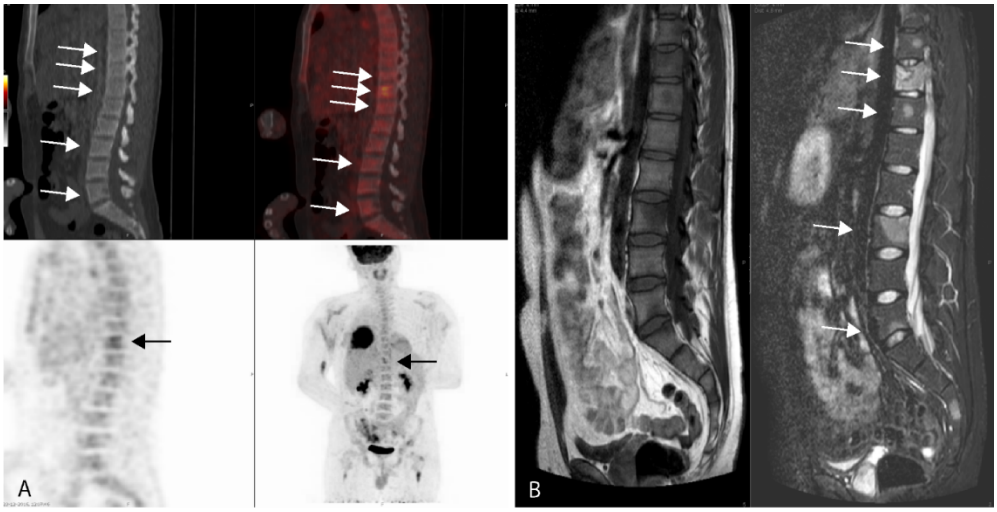

Figure 5 – False-negative lesions on 18F-FDG PET-CT (arrows).
A 23-year-old man presenting with metastatic Ewing sarcoma of the right seventh rib. Images obtained at diagnosis, before the start of treatment. A) 18F-FDG PET-CT showing increased 18F-FDG-uptake at the eleventh thoracic vertebrae only. B) T1-weighted (left) and STIR (right) images showing nodules with a high degree of suspicion for metastasis at the tenth, eleventh, and twelfth thoracic vertebrae and the third and fifth lumbar vertebrae

Discussion

Accurate detection and localization of all metastases in oligometastatic Ewing sarcoma is clinically relevant since metastasectomy or radiation of these sites potentially provides a curative approach. (6)

Of all detected lesions, 95.5% were considered malignant by our reference standard. The PPV of both ^{18}F-FDG PET-CT and MRI are high and the number of false positive lesions low. Thus in this young patient population, any lesion should be considered malignant until proven otherwise. In 39% of confirmed metastases detected with MRI no increased ^{18}F-FDG uptake was present and these were thus missed on ^{18}F-FDG PET-CT. Only two (5%) of these ^{18}F-FDG negative metastases could retrospectively be found by the expert panel on the low dose CT images. On patient basis ^{18}F-FDG PET-CT and MRI both performed well. In only one patient without skeletal metastasis, PET-CT showed inconclusive and thus, according to predefined criteria, false-positive findings, while MRI was true negative. All other patients with suspicion of skeletal metastasis were correctly identified by both imaging modalities. Our results cannot be compared to existing literature, since published reports on performance of MRI relative to ^{18}F-FDG PET-CT are normally based on inclusion of heterogeneous populations with different types of malignancy. In general ^{18}F-FDG PET-CT and MRI are performing well, but there is no consensus in literature about differences in performance in specific tumor types such as Ewing sarcoma.

The question is what can explain the difference between ^{18}F-FDG PET-CT which is based on glucose metabolism within the tumor, and MRI which is based on morphology of metastases in bone marrow. It seems that there are at least three factors that, in combination, are causing these false negatives; activity of normal bone marrow on ^{18}F-FDG PET-CT, small lesion size, and variation in glucose consumption. First, the presence of hematopoietic bone marrow has significant impact on performance of ^{18}F-FDG PET-CT as it decreases contrast between normal and abnormal ^{18}F-FDG uptake. Patients with Ewing sarcomas are young and have active hematopoietic bone marrow in the axial skeleton. Also anemia, previous treatment with chemotherapy or medication may lead to increased activity of hematopoietic marrow in Ewing sarcoma patients. ^{18}F-FDG has an increased uptake in hematopoietic marrow relative to yellow bone marrow, thereby increasing the background activity on ^{18}F-FDG PET-CT. Since hematopoietic bone marrow is typically located in the axial skeleton and proximal extremities, it is no surprise that most (88%) false negative lesions were located in the axial skeleton.

Second, lesion size also contributes to the large number of false-negative lesions on ^{18}F-FDG PET-CT. Ten out of 41 false-negative lesions (24%) were smaller than 10 mm and these smaller lesions were more likely to be false-negative on ^{18}F-FDG PET-CT.

Lastly, changes in the tumor micro-environment of Ewing sarcoma that affect the glucose metabolism may also contribute to the large amount of false-negative lesions of ^{18}F-FDG PET-CT. (20, 21)

This study has a few limitations. First, Ewing sarcoma is a rare disease, so numbers are low. In addition, we performed a retrospective study, so selection bias may play a role: there could have been a reason for the second imaging modality to be performed after the first one (i.e. no independency). Secondly, histopathological confirmation was not available in the majority of the lesions. Follow-up imaging was used as a reference method in the majority of the lesions. Although this is an accepted tool for lesion characterization it could affect the accuracy of our results. Third, imaging analysis was done by one experienced nuclear medicine physician and one experienced radiologist. In general ^{18}F-FDG PET-CT is evaluated by a nuclear medicine physician and MRI by a musculoskeletal (MSK) radiologist. The large number of radiologist allows for more specialization. If two MSK radiologist would have evaluated all imaging data two false-positive lesions (the two bone infarctions in one patients, Figure 1) and two false-negative lesions (that could in retrospect be found on low-dose CT) might have been prevented and could thus be considered as interpretation error. All other lesions did not show ^{18}F-FDG-uptake and were not visible on low-dose CT. Last, in 6 out of 20 cases no whole-body MRI was available for comparison and specificity of both techniques could therefore not be determined. However, there were only three osseous lesions visible on ^{18}F-FDG PET-CT not imaged by MRI.

In conclusion, although no definite conclusions can be drawn from this small retrospective study, we conclude that caution is needed when using ^{18}F-FDG PET-CT for diagnosing skeletal metastases in Ewing sarcoma, since 39% of metastases in this cohort seen on MRI are not detected with ^{18}F-FDG PET-CT. Suggestions of main causes are poor contrast between metastases and active hematopoietic bone marrow small size, and potentially changes in glucose metabolism in metastases of Ewing sarcoma. Further research is needed to evaluate the discrepancy in ^{18}F-FDG PET-CT and MRI findings and confirm our results.

Reference

1. Fletcher CDM, Bridge, J.A., Hogendoorn, P.C.W., Mertens, F. . WHO Classification of Tumours of Soft Tissue and Bone. 4th edition ed. Lyon, France: IARC; 2013.
2. Grunewald TGP, Cidre-Aranaz F, Surdez D, Tomazou EM, de Alava E, Kovar H, et al. Ewing sarcoma. Nat Rev Dis Primers. 2018;4(1):5.
3. Ladenstein R, Potschger U, Le Deley MC, Whelan J, Paulussen M, Oberlin O, et al. Primary disseminated multifocal Ewing sarcoma: results of the Euro-EWING 99 trial. J Clin Oncol. 2010;28(20):3284-91.
4. Gaspar N, Hawkins DS, Dirksen U, Lewis IJ, Ferrari S, Le Deley MC, et al. Ewing Sarcoma: Current Management and Future Approaches Through Collaboration. J Clin Oncol. 2015;33(27):3036-46.
5. Pappo AS, Dirksen U. Rhabdomyosarcoma, Ewing Sarcoma, and Other Round Cell Sarcomas. J Clin Oncol. 2018;36(2):168-79.
6. Haeusler J, Ranft A, Boelling T, Gosheger G, Braun-Munzinger G, Vieth V, et al. The value of local treatment in patients with primary, disseminated, multifocal Ewing sarcoma (PDMES). Cancer. 2010;116(2):443-50.
7. Antoch G, Vogt FM, Freudenberg LS, Nazaradeh F, Goehde SC, Barkhausen J, et al. Whole-body dual-modality PET/CT and whole-body MRI for tumor staging in oncology. JAMA. 2003;290(24):3199-206.
8. Ruggiero A, Lanni V, Librizzi A, Maurizi P, Attina G, Mastrangelo S, et al. Diagnostic Accuracy of 18F-FDG PET/CT in the Staging and Assessment of Response to Chemotherapy in Children With Ewing Sarcoma. J Pediatr Hematol Oncol. 2018;40(4):277-84.
9. Franzius C, Sciuk J, Daldrup-Link HE, Jurgens H, Schober O. FDG-PET for detection of osseous metastases from malignant primary bone tumours: comparison with bone scintigraphy. European journal of nuclear medicine. 2000;27(9):1305-11.
10. Treglia G, Salsano M, Stefanelli A, Mattoli MV, Giordano A, Bonomo L. Diagnostic accuracy of (1)(8)F-FDG-PET and PET/CT in patients with Ewing sarcoma family tumours: a systematic review and a meta-analysis. Skeletal Radiol. 2012;41(3):249-56.
11. Newman EN, Jones RL, Hawkins DS. An evaluation of [F-18]-fluorodeoxy-D-glucose positron emission tomography, bone scan, and bone marrow aspiration/biopsy as staging investigations in Ewing sarcoma. Pediatr Blood Cancer. 2013;60(7):1113-7.
12. Mentzel HJ, Kentouche K, Sauner D, Fleischmann C, Vogt S, Gottschild D, et al. Comparison of whole-body STIR-MRI and 99mTc-methylene-diphosphonate scintigraphy in children with suspected multifocal bone lesions. Eur Radiol. 2004;14(12):2297-302.
13. Daldrup-Link HE, Franzius C, Link TM, Laukamp D, Sciuk J, Jurgens H, et al. Whole-body MR imaging for detection of bone metastases in children and young adults: comparison with skeletal scintigraphy and FDG PET. AJR Am J Roentgenol. 2001;177(1):229-36.
14. Harrison DJ, Parisi MT, Shulkin BL. The Role of (18)F-FDG-PET/CT in Pediatric Sarcoma. Semin Nucl Med. 2017;47(3):229-41.
15. Schmidt GP, Schoenberg SO, Schmid R, Stahl R, Tiling R, Becker CR, et al. Screening for bone metastases: whole-body MRI using a 32-channel system versus dual-modality PET-CT. Eur Radiol. 2007;17(4):939-49.

16. Boellaard R, Delgado-Bolton R, Oyen WJ, Giammarile F, Tatsch K, Eschner W, et al. FDG PET/CT: EANM procedure guidelines for tumour imaging: version 2.0. Eur J Nucl Med Mol Imaging. 2015;42(2):328-54.
17. Salaun PY, Gastinne T, Bodet-Milin C, Campion L, Cambefort P, Moreau A, et al. Analysis of 18F-FDG PET diffuse bone marrow uptake and splenic uptake in staging of Hodgkin's lymphoma: a reflection of disease infiltration or just inflammation? Eur J Nucl Med Mol Imaging. 2009;36(11):1813-21.
18. Inoue K, Goto R, Okada K, Kinomura S, Fukuda H. A bone marrow F-18 FDG uptake exceeding the liver uptake may indicate bone marrow hyperactivity. Ann Nucl Med. 2009;23(7):643-9.
19. Chen Y, Zhou M, Liu J, Huang G. Prognostic Value of Bone Marrow FDG Uptake Pattern of PET/CT in Newly Diagnosed Diffuse Large B-cell Lymphoma. J Cancer. 2018;9(7):1231-8.
20. Blebea JS, Houseni M, Torigian DA, Fan C, Mavi A, Zhuge Y, et al. Structural and functional imaging of normal bone marrow and evaluation of its age-related changes. Semin Nucl Med. 2007;37(3):185-94.
21. Vaupel P, Mayer A. Hypoxia in cancer: significance and impact on clinical outcome. Cancer Metastasis Rev. 2007;26(2):225-39.